

First-Principles Study of Defected Single Layer Hexagonal Boron-Nitride (h-BN)

Hari Krishna Neupane^{1,2} and Narayan Prasad Adhikari^{2*}

¹Amrit Campus, Institute of Science and Technology Tribhuvan University,
Kathmandu, Nepal

²Central Department of Physics, Institute of Science and Technology Tribhuvan University,
Kathmandu, Nepal

*CORRESPONDING AUTHOR:

Narayan Prasad Adhikari

Email: narayan.adhikari@cdp.tu.edu.np

ISSN : 2382-5359(Online),
1994-1412(Print)

DOI:

<https://doi.org/10.3126/njst.v20i2.45775>



Date of Submission: 22/03/2021

Date of Acceptance: 27/01/2022

Copyright: The Author(s) 2021. This is an open access article under the [CC BY](https://creativecommons.org/licenses/by-nc/4.0/) license.



ABSTRACT

The novel properties of pristine h-BN, oxygen (O) atom impurity defects in h-BN (h-B(N-O) and h-(B-O) N), one boron (1B) atom vacancy defect in h-BN (h-BN_1B) and one nitrogen (1N) atom vacancy defect in h-BN (h-BN_1N) materials are investigated by spin-polarized density functional theory (DFT) using computational tool Quantum ESPRESSO. We found that they are stable materials. From the band structure calculations, we found that all the considered systems are wide bandgap materials. The bandgap energy of pristine h-BN, impurity defects h-B(N-O) and h-(B-O) N, and vacancy defects h-BN_1B and h-BN_1N materials have values 4.98 eV, 4.19 eV & 2.47 eV, and 4.84 eV & 3.62 eV respectively. Also, it is found that h-B(N-O) and h-BN_1N materials have n-type Schottky contact while h-(B-O)N and h-BN_1B materials have p-type Schottky contact. From the analysis of density of states (DOS) and partial density of states (PDOS) calculations, we found that non-magnetic pristine h-BN changes to magnetic h-B(N-O) and h-(B-O) N materials due to presence of impurity defects, and h-BN_1B and h-BN_1N materials due to presence of vacancy defects. Magnetic moments of h-B(N-O), h-(B-O)N, h-BN_1B and h-BN_1N materials are 1.00 μ_B /cell, 0.94 μ_B /cell, 3.00 μ_B /cell and 1.00 μ_B /cell respectively. They are obtained due to unpaired up and down spins state of electrons in 2p orbital of B and N atoms in the structures.

Keywords: DFT, Impurity, Vacancy, Defects, Magnetic moment

1. INTRODUCTION

Two dimensional (2D) materials like graphene (G), hexagonal Boron-Nitride (h-BN), Molybdenum diSulphide (MoS_2) are attracting candidates for electronic and optoelectronic devices because of their excellent physical properties (Geim & Novoselov 2007; Song *et al.* 2010; Wang *et al.* 2012; Wangs *et al.* 2014; Zhang *et al.* 2016; Tran *et al.* 2016). Similar like hexagonal structure of graphene (Neupane & Adhikari 2020; Neupane & Adhikari 2021), Boron (B) atoms and Nitrogen (N) atoms of 2D h-BN are alternately arranged to form smooth surface hexagonal honeycomb lattice structure (Neupane & Adhikari 2021). 2D h-BN has a large optical phonon mode, no dangling bonds on the surface and has wide bandgap energy of value 5.80 eV (Watanabe *et al.* 2004), called wide bandgap class of materials (insulators). The bond length of B-N atoms is 1.45Å (Lynch & Drickamer 1996), which is formed through sp^2 -hybridization. In layered structures, B atoms and N atoms are joined by covalent bonds in each layer, and adjacent layers of h-BN are combined with weak van der Waals (vdW) forces (Jin *et al.* 2009; Nag *et al.* 2010; Le 2014). The h-BN has well known mechanical properties such as Young's modulus ~270 Nm⁻², thermal conductivity at room temperature 300 Wm⁻¹K⁻¹, and tensile strength 41 MPa (Zhou *et al.* 2007; Zhi *et al.* 2009; Zhou *et al.* 2014). 2D pristine and defected h-BN crystal structures are studied by both theoretical and experimental research groups and found that it has no absorption in the visible range, but it has absorption spectroscopy in the ultraviolet region and a good photo luminescence property (Jaffrennou *et al.* 2007; Museur *et al.* 2008; Wirtz & Rubio 2009). The non-magnetic nature of 2D h-BN limits its practical applications in widely expanding field of devices applications. Researchers (Wu *et al.* 2005; Si & Xue 2007)

found that impurity (doping) and vacancy defects in 2D h-BN have unprompted spin magnetization. Therefore, defected h-BN presents exemplary half-metallic magnetism in a variety of states. The magnetic properties of materials have great attractive properties because magnetic materials are used in the fields of biomedicine, molecular biology, biochemistry, diagnosis, catalysis, nanoelectronic devices and various other industrial applications (Makarova *et al.* 2019; Peng *et al.* 2016). To our best knowledge, structural, electronic and magnetic properties of h-BN supercell structure due to the oxygen atom impurity defects, boron atom vacancy defects and nitrogen atom vacancy defects have not been reported. Therefore, in this paper, we investigated structural, electronic, and magnetic properties of impurity defects [nitrogen atom is replaced by oxygen atom in pristine (4×4) supercell h-BN structure i.e. h-B(N-O) and boron atom is replaced by oxygen atom in pristine (4×4) supercell h-BN structure i.e. h-(B-O)N], and 1B atom vacancy defects (h-BN_1B), 1N atom vacancy defects (h-BN_1N) materials in (4×4) supercell structure of h-BN through first-principles calculations by using spin-polarized density functional theory (SDFT). The computational tool used is Quantum ESPRESSO (QE) code.

2. COMPUTATIONAL METHODS

We performed first-principles calculations to study structural, electronic and magnetic properties of Oxygen atom impurity defects, 1B atom vacancy defects and 1N atom vacancy defects materials respectively in (4×4) supercell structure of h-BN, based on the spin-polarized density functional theory (SDFT) approach (Hohenberg & Kohn 1964) by using Quantum ESPRESSO (QE) computational package (Giannozzi *et al.* 2009). The electronic exchange and correlation effects in the systems were treated by Generalized Gradient Approximation

(GGA) using Perdew-Burke-Ernzerhof (PBE) (Perdew *et al.* 1996). Among the various types of pseudo-potentials, we used Rappe-Rabe-Kaxiraas-Joannopoulos (RRKJ) model of ultra-soft pseudo-potentials to explain the chemically active valence electrons in all calculations. The Broyden-Fletcher-Goldfarb-Shanno (BFGS) algorithm (Pfrommer *et al.* 1997) was used to relax the structures until the total energy changes was less than 10^{-4} Ry between two consecutive self-consistent field (SCF) steps and each component of force acting was less than 10^{-3} Ry/Bohrs to get geometrically optimized structures. The unit cell was optimized with respect to lattice parameter, kinetic energy cut-off for plane-wave and the number of k-points along 'x' and 'y' axes respectively. We have obtained the values of lattice constant ($a = 2.49 \text{ \AA}$), kinetic energy cut-off ($E_{\text{cut}} = 40 \text{ Ry}$), charge density cut-off ($\rho = 400 \text{ Ry}$), and a mesh of $(20 \times 20 \times 1)$ k-points of Boron-Nitride (B-N) unit cell from the convergence test. This mesh was obtained from the plot of total energy versus number of k-points, which was used for the Brillouin zone integration. In (4×4) supercell structure of h-BN, the lattice constant was four times that of unit cell and a mesh of k-points was reduced to $(6 \times 6 \times 1)$. The reduction of mesh was due to the relation of direct and reciprocal lattice geometries. The Marzari-Vanderbilt (MV) (Marzari *et al.* 1999) method of smearing with a small width of 0.001 Ry was used. Moreover, we have chosen 'david' diagonalization method with 'plain' mixing mode and mixing factor of 0.7 for self-consistency. Spin-polarized DFT calculations were used to study the magnetic properties of the systems. For band structure calculations, 100 k-points were chosen along the high symmetric points connecting the reciprocal space. For the density of states (DOS) and partial density of states (PDOS) calculations, we used denser mesh of $(12 \times 12 \times 1)$ k-points.

In present work, we have constructed impurity defects h-B(N-O) and h-(B-O) N, materials, where 1N atom and 1B atom respectively replaced by 1O atom in h-BN supercell structure. The vacancy defects h-BN_1B and h-BN_1N materials were prepared by removing 1B atom and 1N atom separately from the (4×4) supercell structure of h-BN. These prepared impurity and vacancy defects structures were then optimized and relaxed by using BFGS scheme. They were used for further calculations as shown in fig. 1.

Finding were obtained from band structure, density of states (DOS) and partial density of states (PDOS) calculations of impurity and vacancy defects materials. Analysis of calculations was done based on spin-polarized DFT method using QE code.

3. RESULTS AND DISCUSSION

3.1 Structural and Electronic Properties

The (4×4) supercell structure of h-BN was obtained by continuing optimized primitive unit cell along x and y directions. The bond length of B-N atoms was found 1.44 \AA , and B-B atoms found 2.49 \AA , these values agreed with reported values 1.45 \AA (Lynch & Drickamer 1996) and 2.50 \AA (Sponza *et al.* 2018) respectively. The h-BN structure has no dangling bonds on its surface. Hence, it's smoothest surface reduced chemical activity. The impurity defects h-B(N-O) and h-(B-O) N materials were prepared by substituting 1O atom in place of 1N and 1B atoms respectively in pristine h-BN structure as shown in fig. 1(b-c), and vacancy defects h-BN_1B and h-BN_1N materials were constructed by removing 1B and 1N atoms separately from pristine h-BN structure as shown in fig. 1(c-d). The prepared structures were relaxed using BFGS method (Pfrommer *et al.* 1997) and found that they were stable for further calculations as shown in fig. 1(b-e).

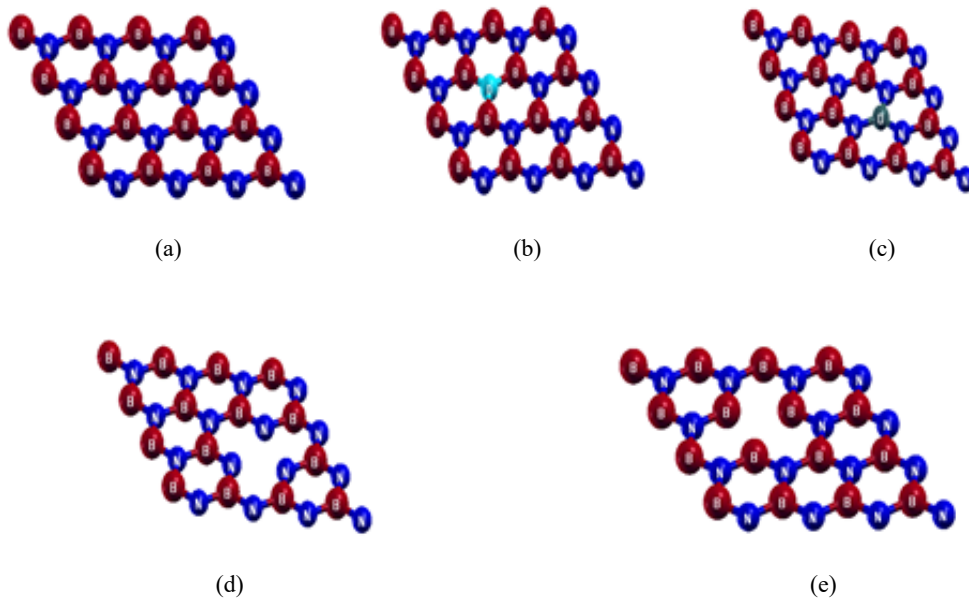


Fig. 1: Optimized and relaxed stable structures of pristine, impurity defects and vacancy defects material of hexagonal Boron-Nitride (a) (4×4) supercell structure of monolayer h-BN (b) 1O atom impurity defects in (4×4) supercell structure of h-BN where 1N atom was replaced by 1O atom (c) 1O atom impurity defects in (4×4) supercell structure of h-BN where 1B atom was replaced by 1O atom (d) 1B atom vacancy defects in (4×4) supercell structure of h-BN (e) 1N atom vacancy defects in (4×4) supercell structure of h-BN.

The stability of the structures was determined by calculating total energy of the systems, which are given in table 1.

Table 1: Fermi energy (E_f), Fermi energy shift (E_s), bandgap energy (E_g) and total energy (E_t) of pristine h-BN and defected h-BN materials

Pristine h-BN & defected h-BN materials	(E_f) eV	(E_s) eV	(E_g) eV	(E_t) Ry
h-BN	-3.2	-	4.98	-239.97
h-B(N-O) impurity defect	0.35	3.55	4.19	-251.91
h-(B-O)N impurity defect	-1.03	2.17	2.47	-265.23
h-BN_1B vacancy defect	-4.12	-0.92	4.84	-232.94
h-BN_1N vacancy defect	-0.95	2.25	3.62	-219.19

Total energy of the system was obtained by the sum of one-electron contributions, Hartree contribution, exchange-correlation contribution, Ewald contribution and smearing contribution. These values were obtained from SCF calculations. Higher the value of total energy, more stable was the system. Thus, order of total energy of structures was found to be as h-(B-O)N > h-B(N-O) > h-BN > h-BN_1B > h-BN_1N.

The electronic properties of materials were investigated from the analysis of electronic

band structure and DOS calculations. The band structures and DOS plots of h-BN, h-B(N-O), h-(B-O)N, h-BN_1B and h-BN_1N materials were shown in figures 2(a-b), 3(a-b), 4(a-b), 5(a-b) and 6(a-b) respectively. In band structure plots, 100 k-points were taken along the specific direction of irreducible Brillouin zone by choosing Γ -M-K- Γ high symmetric points, where x-axis represents high symmetric points in the first Brillouin zone and y-axis represents the corresponding energy value. In DOS plots, up and down spins states

of electrons were plotted along y-axis and its corresponding energy values was given in x-axis, also the vertical dotted line represents Fermi energy level and horizontal dotted line separates up and down spins states of electrons in the orbital of all atoms present in structures. We know that electronic configurations of valence electrons of B, N and O atoms present in pristine h-BN and defected materials were $[\text{He}] 2s^2 2p^1$, $[\text{He}] 2s^2 2p^3$ and $[\text{He}] 2s^2 2p^4$ respectively. Each B atom has single up spin in $2p_x$ and vacant in $2p_y$ and $2p_z$ sub-orbital, each N atom has one unpaired up spin in each p_x , p_y and p_z sub-orbital. Similarly, O atom contains paired spins in $2p_x$ sub-orbital and single unpaired up spin in $2p_y$ and $2p_z$ sub-orbital. Before studying the electronic properties of h-B(N-O), h-(B-O)N, h-BN_1B and h-BN_1N materials, we first need to understand the electronic properties

of pristine h-BN. We have done electronic band structures calculations of (4×4) supercell structure of h-BN, it is found that values of p-type and n-type Schottky barrier heights are 0.98 eV and 3.99 eV respectively as shown in figure 2(a). We know that sum of n-type Schottky barrier height and p-type Schottky barrier height gives energy bandgap of the semiconductors/insulators materials (Chen *et al.* 2013; Hu *et al.* 2016). Thus, bandgap energy value of h-BN has 4.98 eV, which was close with reported value (Watanabe *et al.* 2004). Also, we have analyzed the DOS plot of h-BN as shown in figure 2(b) and found that unoccupied up and down spins states of electrons are present at 0.99 eV energy value below in valence band and 3.99 eV energy value above in conduction band from the Fermi energy level. Hence, h-BN is a p-type wide bandgap material.

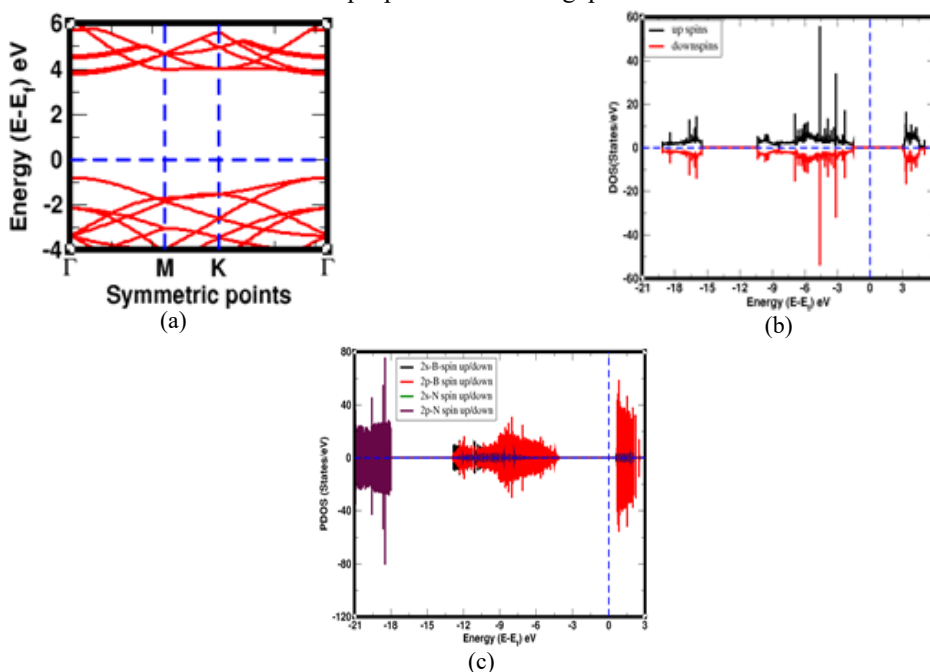


Fig. 2: (a) Band structure of up and down spins states of monolayer h-BN material (b) DOS of up and down spins states of atoms in h-BN material (c) PDOS of individual up and down spins states of all atoms in h-BN. In band structure, horizontal dotted line represents Fermi energy level, and in DOS and PDOS plots, vertical dotted line represents Fermi energy level.

In addition, to study electronic properties of h-B(N-O), h-(B-O)N, h-BN_1B and h-BN_1N materials, we have analyzed band structures and DOS plots are illustrated in fig. 3(a-b), 4(a-b), 5(a-b) and 6(a-b) respectively. We found that Fermi energy values and Fermi shift energy values of h-B(N-O), h-(B-O)N, h-BN_1B, h-BN_1N materials are +0.35

eV, -1.03 eV, -4.12 eV, -0.95 eV and +3.55 eV, +2.17 eV, -0.92 eV, +2.25 eV respectively. These unequal energies values are obtained due to unpaired up and down spins states of electrons in the sub-orbitals of atoms of impurity and vacancy defects structures. We observed the electronic band structure and DOS plot of h-B(N-O) material, and found that up spins

of electronic bands appear around the Fermi energy level, and states of down spins electronic bands open bandgap in conduction band. But, both up and down spins states of electronic bands have open bandgap in valence band as shown in fig. 3(a). This is because; numbers of electrons are increased in h-B(N-O) material due to the replacement of pentavalent 1N atom by 1O impurity atom. Also, in DOS plot, up spin states are appeared in the Fermi level and down spins states were shifted little distance towards the conduction band, but both spins states opened energy bandgap in structure as shown in fig. 3(b). Therefore, from band structure and DOS analysis, we concluded that n-type Schottky contact h-B(N-O) material has bandgap energy of value 4.19eV. On the other hand, trivalent 1B atom is replaced by 1O impurity atom in h-(B-O)N structure. We found that electronic bands of down spin states cross the Fermi energy level, and up spin electronic bands appear around the Fermi level in valence band. These both spins states developed energy bandgap in conduction band as shown in fig. 4(a). Also, we studied DOS plot of h-(B-O)N, and found that both up and down spins states create electronic bandgap as shown in figure 4(b). Hence, from band and DOS calculations, we conclude that p-type Schottky contact material

h-(B-O)N obtained energy bandgap of value 2.47 eV. Similarly, we have analyzed band structures and DOS plots of h-BN_1B and h-BN_1N materials. In band structure, it is seen that electronic band states due to down spins of electrons are appeared around the Fermi energy level and up spins states appeared little distance below the Fermi level in valence band of h-BN_1B material as shown in fig. 5(a). Electronic states of both spins made bandgap in conduction band. Similar results are obtained in DOS plot as shown in fig. 5(b). Hence, from band and DOS calculations, we conclude that p-type Schottky contact h-BN_1B material opened electronic bandgap of energy value 4.84 eV. On the other hand, we have studied band structure and DOS plot of up and down electronic states of h-BN_1N material as shown in fig. 6(a-b). It was found that both spins states obtained energy bandgap of value 3.62 eV. Hence, h-BN_1N was called n-type Schottky contact wide bandgap material. Therefore, from the band structures and DOS plots calculations of impurity and vacancy defects materials, we found that h-(B-O)N and h-BN_1B are wide bandgap p-type Schottky contact materials, and h-B(N-O) and h-BN_1N are wide bandgap n-type Schottky contact materials.

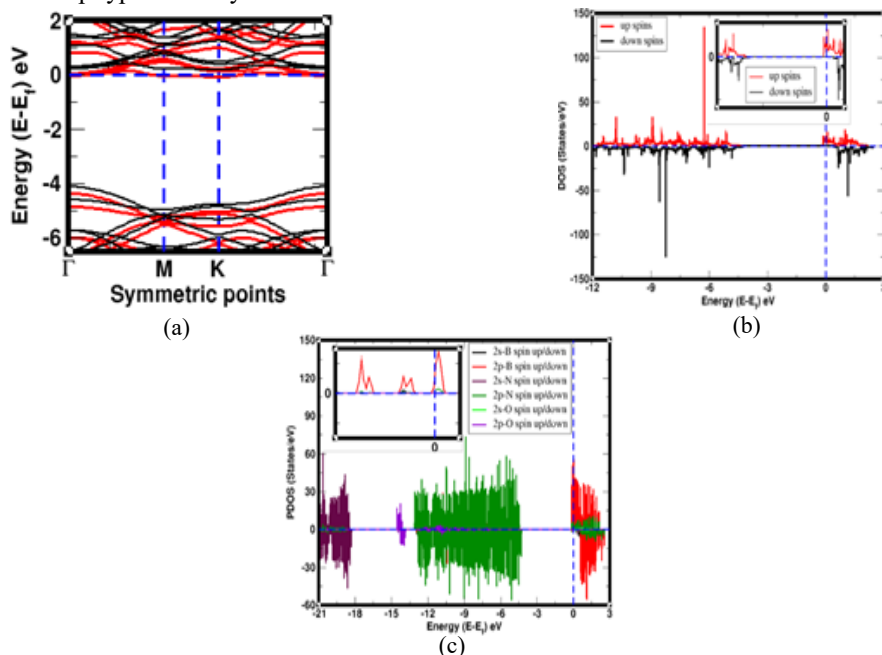


Fig. 3: (a) Band structure of up and down spins states of 1O impurity defects h-BN material, where red colour of bands represent up spin states and black colour of bands represent down spin states (b) DOS of up and down spins states of atoms in 1O impurity defects h-BN, where 1N atom was replaced by 1O atom in structure (c) PDOS of individual up and down spins states of all atoms in 1O impurity defects h-BN, where 1N atom is replaced by 1O atom in structure. In band structure, horizontal dotted line represents Fermi energy level, and in DOS and PDOS plots, vertical dotted line represents Fermi energy level. In DOS and PDOS plots, insets represent the zoom in the scale near the Fermi energy.

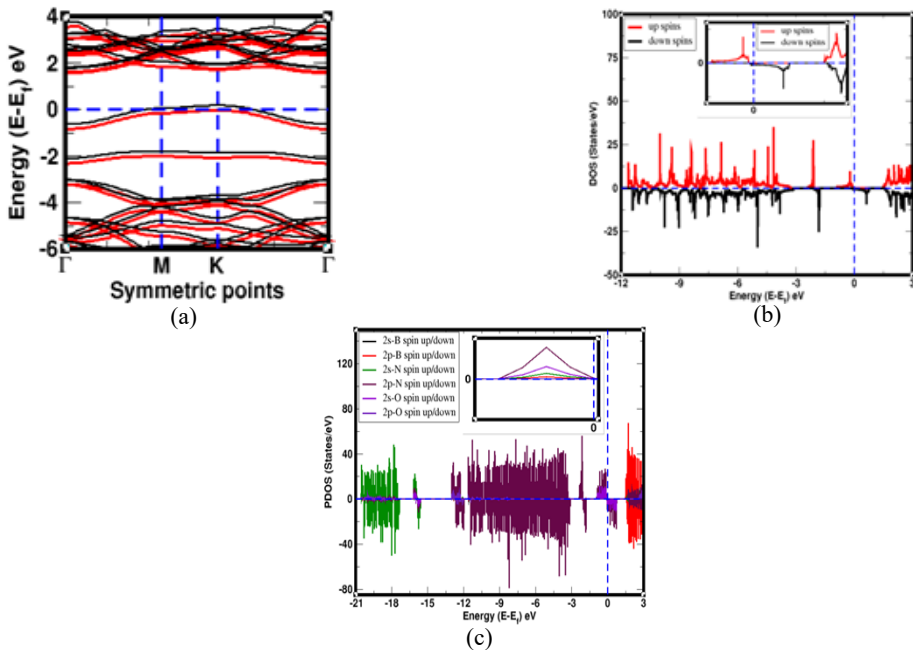


Fig. 4: (a) Band structure of up and down spins states of IO impurity defects h-BN material, where red colour of bands represent up spin states and black colour of bands represent down spin states (b) DOS of up and down spins states of atoms in IO impurity defects h-BN, where 1B atom was replaced by IO atom in structure (c) PDOS of individual up and down spins states of all atoms in IO impurity defects h-BN, where 1B atom is replaced by IO atom in structure. In band structure, horizontal dotted line represents Fermi energy level, and in DOS and PDOS plots, vertical dotted line represents Fermi energy level. In DOS and PDOS plots, insets represent the zoom in the scale near the Fermi energy.

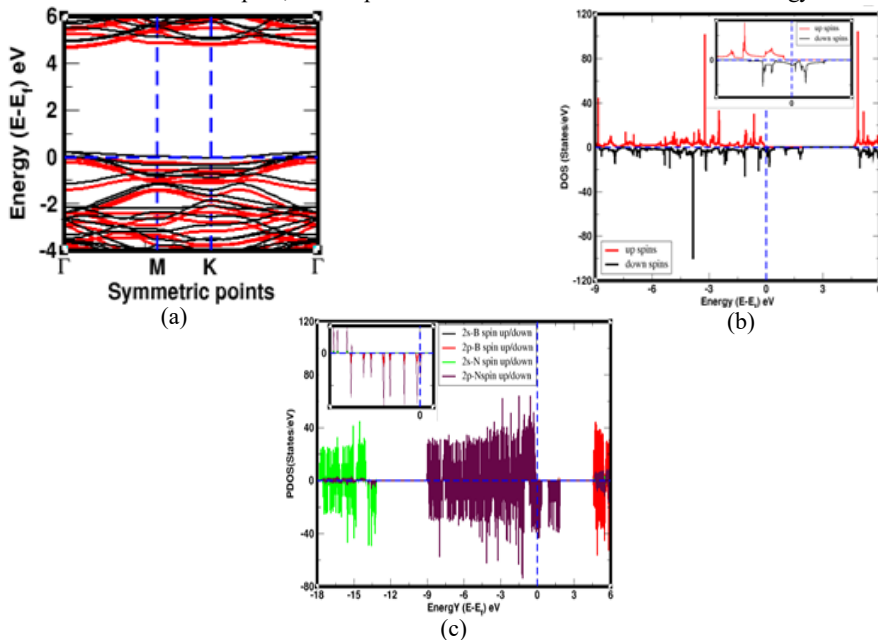


Fig. 5: (a) Band structure of up and down spins states of 1B atom vacancy defects in h-BN material, where red colour of bands represent up spin states and black colour of bands represent down spin states (b) DOS of up and down spins states of 1B atom vacancy defects in h-BN (c) PDOS of individual up and down spins states of all atoms in 1B atom vacancy defects h-BN. In band structure, horizontal dotted line represents Fermi energy level, and in DOS and PDOS plots, vertical dotted line represents Fermi energy level. In DOS and PDOS plots, insets represent the zoom in the scale near the Fermi energy.

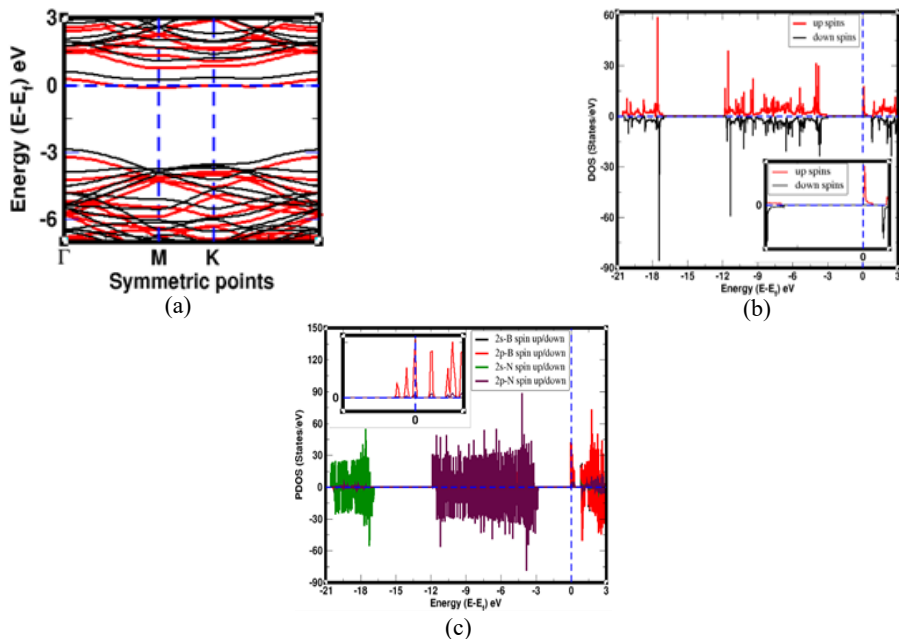


Fig. 6: (a) Band structure of up and down spins states of 1N atom vacancy defects in h-BN material, where red colour of bands represent up spin states and black colour of bands represent down spin states (b) DOS of up and down spins states of 1N atom vacancy defects in h-BN (c) PDOS of individual up and down spins states of all atoms in 1N atom vacancy defects h-BN. In band structure, horizontal dotted line represents Fermi energy level, and in DOS and PDOS plots, vertical dotted line represents Fermi energy level. In DOS and PDOS plots, insets represent the zoom in the scale near the Fermi energy

3.2 Magnetic Properties

Magnetic properties of materials was obtained by the analysis of DOS and PDOS calculations. The asymmetrically distributed up and down spins states of electrons in DOS and PDOS plots means, materials have magnetic properties, and symmetrically distributed up and down spins states of electrons in DOS and PDOS reveals that materials carry non-magnetic properties. It was

found that DOS/PDOS up and down spins states of electrons in the orbitals of B and N atoms of h-BN structure was symmetrically distributed as shown in figures 2(b-c). The net magnetic moment was given by up and down spin states of electrons in 2s, 2p orbitals of B and N atoms in structure have $0.00\mu_B/\text{cell}$, and it was given in table 2. Hence, h-BN material has non-magnetic properties.

Table 2: Magnetic moment due to total up and down spins of electrons (μ) in 2s and 2p orbitals of B and N atoms in pristine h-BN, 1B atom vacancy defects h-BN (h-BN_1B), 1N atom vacancy defects h-BN (h-BN_1N) materials and 2s and 2p orbitals of B, N and O atoms in impurity defected h-B(N-O) and h-(B-O)N materials.

Magnetic moment calculations					
of h-BN, h-B(N-O), h-(B-O)N, h-BN_1B & h-BN_1N materials	h-BN μ_B/cell	h-B(N-O) μ_B/cell	h-(B-O)N μ_B/cell	h-BN_1B μ_B/cell	h-BN_1N μ_B/cell
μ -due to 2s of B atoms (μ_B/cell)	0	0.03	0	0.02	0.02
μ -due to 2p of B atoms (μ_B/cell)	0	0.64	0.06	0.84	0.78
μ -due to 2s of N atoms (μ_B/cell)	0	0.02	0.08	0.22	0.02
μ -due to 2p of N atoms (μ_B/cell)	0	0.31	0.74	1.92	0.18
μ -due to 2s of O atoms (μ_B/cell)	-	0	0	-	-
μ -due to 2p of O atom (μ_B/cell)	-	0	0.06	0	-
Total value of magnetic moment M(μ_B/cell)	0	1	0.94	3	1

Furthermore, we have investigated the magnetic properties of h-B(N-O), h-(B-O)N, h-BN_1B and h-BN_1N materials by using DOS and PDOS analysis. DOS and PDOS plots of above respective materials were illustrated in figures 3(b-c), 4(b-c), 5(b-c) and 6(b-c) respectively, where up and down spins states of DOS and PDOS are plotted along y-axis and its corresponding energy values were given in x-axis, also the vertical dotted line represents Fermi energy level and horizontal dotted line separates up and down spins states of electrons in the orbital of all atoms present in studied materials. We observed that up and down spin states of electrons in 2s, 2p orbitals of B and N atoms were asymmetrically (unequal) distributed in h-BN_1B and h-BN_1N materials, where unequally distributed up and down spins states of electrons present around the Fermi energy level because electron's spins degeneracy of the bands due to 1B atom vacancy defects in h-BN_1B and 1N atom vacancy defects in h-BN_1N, bands are broken and splitted. As a result, h-BN_1B and h-BN_1N materials bear magnetic properties. We have calculated the magnetic moments given by spins of electrons in 2s, 2p orbitals of B have values 0.02 $\mu\text{B}/\text{cell}$, 0.84 $\mu\text{B}/\text{cell}$ and N atoms have values 0.22 $\mu\text{B}/\text{cell}$, 1.92 $\mu\text{B}/\text{cell}$ respectively in h-BN_1B. And 2s, 2p orbitals of B atoms have values 0.02 $\mu\text{B}/\text{cell}$, 0.78 $\mu\text{B}/\text{cell}$ and 2s, 2p orbitals of N atoms have values 0.02 $\mu\text{B}/\text{cell}$, 0.18 $\mu\text{B}/\text{cell}$ respectively in h-BN_1N. Hence, total magnetic moment values of h-BN_1B and h-BN_1N materials are 3.00 $\mu\text{B}/\text{cell}$ and 1.00 $\mu\text{B}/\text{cell}$ respectively. Similarly, the spins states of electrons in the orbital of B, N and O atoms of h-B(N-O), h-(B-O)N materials near the Fermi energy level are asymmetrically distributed in DOS and PDOS plots as shown in figures 3(b-c) and 4(b-c) respectively. Magnetic moments are given by spins states of electrons in 2s, 2p orbitals of B atoms; 2s, 2p orbitals of N atoms; 2s, 2p orbitals of O atoms in h-B(N-O) and h-(B-O) N structures have values 0.03 $\mu\text{B}/\text{cell}$, 0.64 $\mu\text{B}/\text{cell}$; 0.02 $\mu\text{B}/\text{cell}$, 0.31 $\mu\text{B}/\text{cell}$; 0.00 $\mu\text{B}/\text{cell}$, 0.00 $\mu\text{B}/\text{cell}$ and 0.00 $\mu\text{B}/\text{cell}$, 0.06 $\mu\text{B}/\text{cell}$; 0.08

$\mu\text{B}/\text{cell}$, 0.74 $\mu\text{B}/\text{cell}$; 0.00 $\mu\text{B}/\text{cell}$, 0.06 $\mu\text{B}/\text{cell}$ respectively. Therefore, total values of magnetic moment of h-B(N-O) and p h-(B-O)N materials are 1.00 $\mu\text{B}/\text{cell}$ and 0.94 $\mu\text{B}/\text{cell}$ respectively. Hence, h-B(N-O) and h-(B-O)N materials have magnetic properties. From above calculations, magnetic moments of vacancy defects materials are greater than impurity defects materials. This was because; unequal dangling bonds are formed due to the effects of 1B & 1N vacancy defects atoms in structures.

4. CONCLUSION

The structural, electronic and magnetic properties of oxygen atom impurity defects in h-BN (h-B(N-O) and h-(B-O)N) materials, one boron atom vacancy defect in h-BN (h-BN_1B) and one nitrogen atom vacancy defect in h-BN (h-BN_1N) materials have been investigated by first-principles calculations based on spin-polarized DFT method using computational tool Quantum ESPRESSO code. From the structural analysis, we found that pristine h-BN and defected h-B(N-O), h-(B-O)N, h-BN_1B, h-BN_1N are stable materials. We have studied the electronic properties of pristine and defected h-BN material by analyzing their band structures and density of states (DOS) calculations, and found that h-BN, h-B(N-O), h-(B-O)N, h-BN_1B and h-BN_1N materials have open energy bandgap of values 4.98 eV, 4.19 eV, 2.47 eV, 4.84 eV and 3.62 eV respectively. Therefore, they was called wide bandgap materials. Also, it was found that h-B(N-O) and h-BN_1N materials have n-type Schottky contact and h-(B-O)N and h-BN_1B materials have p-type Schottky contact. In addition, we have carried out density of states (DOS) and partial density of states (PDOS) calculations and found that h-B(N-O), h-(B-O)N, h-BN_1B and h-BN_1N are magnetic materials. Thus, non-magnetic pristine h-BN material changes to magnetic h-B(N-O), h-(B-O) N materials by O atom impurity defects in h-BN, and h-BN_1B, h-BN_1N materials due to the 1B atom and 1N atom vacancy defects in h-BN respectively. We have calculated the magnetic

moments of h-B(N-O), h-(B-O)N, h-BN_1B and h-BN_1N, they are 1.00 $\mu\text{B}/\text{cell}$, 0.94 $\mu\text{B}/\text{cell}$, 3.00 $\mu\text{B}/\text{cell}$ and 1.00 $\mu\text{B}/\text{cell}$ respectively. High value of magnetic moments was contributed by unpaired spin states of electrons in the sub-orbitals of 2p orbital of B and N atoms in structures.

ACKNOWLEDGEMENT

Hari Krishna Neupane and Narayan Prasad Adhikari acknowledge to UGC Nepal, PhD grants of award no. PhD-75/76-S &T-09 and UGC grants CRG 073/74 -S&T -01 respectively. Also, Narayan Prasad Adhikari acknowledges to network project NT-14 of ICTP/OEA

REFERENCES

- Chen, W., E. J. Santos, W. Zhu, E. Kaxiras and Z. Zhang. (2013). Tuning the electronic and chemical properties of monolayer MoS₂ adsorbed on transition metalsubstrates. *Nano letters*, 13(2), 509-514.
- Geim, A. K. and K. S. Novoselov. (2007). The rise of graphene. *Nature Materials*, 6(3), 183-191.
- Giannozzi, P., S. Baroni, N. Bonini, M. Calandra, R. Car, C. Cavazzoni and A. Dal Corso. (2009). QUANTUM ESPRESSO: modular and open-source software Project for quantum simulations of materials. *Journal of physics: Condensed Matter*, 21(39), 395502.
- Hohenberg, P. and W. Kohn. (1964). Inhomogeneous electron gas. *Physical Review*, 136(3B), B864.
- Hu, W., T. Wang, R. Zhang and J. Yang. (2016). Effects of interlayer coupling and electric fields on the electronic structures of graphene and MoS₂ heterobilayers. *Journal of Materials Chemistry C*, 4(9), 1776-1781.
- Jaffrennou, P., J. Barjon, J. S. Lauret, B. Attal-Trétout, F. Ducastelle and A. Loiseau. (2007). Origin of the excitonic recombinations in hexagonal boron nitride by spatially resolved cathodo luminescence spectroscopy.
- Jin, C., F. Lin, K. Suenaga and S. Iijima. (2009). Fabrication of a freestanding boron nitride single layer and its defect assignments. *Physical review letters*, 102(19), 195505.
- Le, M. Q. (2014). Size effects in mechanical properties of boron nitride nanoribbons. *Journal of Mechanical Science and Technology*, 28(10), 4173-4178.
- Lynch, R. W. and H. G. Drickamer. (1966). Effect of high pressure on the lattice parameters of diamond, graphite, and hexagonal boron nitride. *The Journal of Chemical Physics*, 44(1), 181-184.
- Makarova, M. V., Y. Akaishi, T. Ikarashi, K. S. Rao, S. Yoshimura and H. Saito. (2019). Alternating Magnetic Force Microscopy: Effect of Si doping on the temporal performance degradation of amorphous FeCoB magnetic tips. *Journal of Magnetism and Magnetic Materials*, 471, 209-214.
- Marzari, N., D. Vanderbilt, A. De Vita and M. C. Payne. (1999). Thermal Contraction and disordering of the Al (110) surface. *Physical review Letters*, 82(16), 3296.
- Museur, L., E. Feldbach and A. Kanaev. (2008). Defect-related photoluminescence of hexagonal boron nitride. *Physical review B*, 78(15), 155204.
- Nag, A., K. Raidongia, K. P. Hembam, R. Datta, U. V. Waghmare and C. N. R. Rao. (2010). Graphene analogues of BN: novel synthesis and properties. *ACS nano*, 4(3), 1539-1544.
- Neupane, H. K. and N. P. Adhikari. (2020). Structure, electronic and magnetic properties of 2D Graphene-Molybdenum disulfide (G-MoS₂) Heterostructure(HS) with vacancy defects at Mo sites. *Computational Condensed Matter*, e00489.
- Neupane, H. K. and N. P. Adhikari. (2020). Tuning Structural, Electronic, and Magnetic

- Properties of C Sites Vacancy Defects in Graphene/MoS₂ van der Waals Heterostructure Materials: A First-Principles Study. *Advances in Condensed Matter Physics*, 2020.
16. Neupane, H. K. & N. P. Adhikari. (2021). First-principles study of structure, electronic, and magnetic properties of C sites vacancy defects in water adsorbed graphene/MoS₂ van der Waals heterostructures. *Journal of Molecular Modeling*, 27(3), 1-12.
 17. Neupane, H. K. and N. P. Adhikari. (2021). Effect of vacancy defects in 2D vdW-graphene/h-BN heterostructure: First-principles study. *AIP Advances*, 11(8), 085218.
 18. Peng, H. X., F. Qin and M. H. Phan. (2016). Ferromagnetic microwire composites: from Sensors to microwave applications. Springer.
 19. Perdew, J. P., K. Burke and M. Ernzerhof. (1996). Generalized gradient approximation made simple. *Physical review letters*, 77(18), 3865.
 20. Pfrommer, B. G., M. Côté, S. G. Louie and M. L. Cohen. (1997). Relaxation of Crystals with the quasi-Newton method. *Journal of Computational Physics*, 131(1), 233-240.
 21. Si, M. S. and D. S. Xue. (2007). Magnetic properties of vacancies in a graphitic boron nitride sheet by first-principles pseudopotential calculations. *Physical Review B*, 75(19), 193409.
 22. Song, L., L. Ci, H. Lu, P. B. Sorokin, C. Jin, J. Ni and P. M. Ajayan. (2010).
 23. Sponza, L., H. Amara, C. Attacalite, S. Latil, T. Galvani, F. Paleari and F. Ducastelle. (2018). Direct and indirect excitons in boron nitride polymorphs: A story of atomic configuration and electronic correlation. *Physical Review B*, 98(12), 125206.
 24. Large scale growth and characterization of atomic hexagonal boron nitride layers. *Nano letters*, 10(8), 3209-3215.
 25. Tran, T. T., K. Bray, M. J. Ford, M. Toth and I. Aharonovich. (2016). Quantum emission from hexagonal boron nitride monolayers. *Nature nanotechnology*, 11(1), 37-41.
 26. Wang, Q. H., K. Kalantar-Zadeh, A. Kis, J. N. Coleman and M. S. Strano. (2012). Electronics and optoelectronics of two-dimensional transition metal dichalcogenides. *Nature nanotechnology*, 7(11), 699-712.
 27. Wang, H., H. Feng and J. Li. (2014). Graphene and graphene-like layered transition metal dichalcogenides in energy conversion and storage. *Small*, 10(11), 2165-2181.
 28. Watanabe, K., T. Taniguchi and H. Kanda. (2004). Direct-bandgap properties and evidence for ultraviolet lasing of hexagonal boron nitride single crystal. *Nature materials*, 3(6), 404-409.
 29. Wirtz, L. and A. Rubio. (2009). Optical and vibrational properties of boron nitride nanotubes. In *BCN Nanotubes and Related Nanostructures* (pp. 105-148). Springer, New York, NY.
 30. Wu, R. Q., L. Liu, G. W. Peng and Y. P. Feng. (2005). Magnetism in BN nanotubes induced by carbon doping. *Applied physics letters*, 86(12), 122510.
 31. Wu, R. Q., G. W. Peng, L. Liu and Y. P. Feng. (2005). Possible graphitic-boron-nitride-based metal-free molecular magnets from first principles study. *Journal of Physics: Condensed Matter*, 18(2), 569.
 32. Zhang, S., M. Xie, F. Li, Z. Yan, Y. Li, E. Kan and H. Zeng. (2016). Semiconducting group 15 monolayers: a broad range of band gaps and high carrier mobilities. *Angewandte Chemie*, 128(5), 1698-1701.
 33. Zhi, C., Y. Bando, C. Tang, H. Kuwahara and D. Golberg. (2009). Large-scale fabrication of boron nitride nanosheets and their utilization in polymeric composites with improved thermal and mechanical properties. *Advanced Materials*, 21(28), 2889-2893.

34. Zhou, H., J. Zhu, Z. Liu, Z. Yan, X. Fan, J. Lin and J. M. Tour. (2014). Highthermal conductivity of suspended few-layer hexagonal boron nitride sheets. *NanoResearch*, 7(8), 1232-1240.
35. Zhou, W., S. Qi, Q. An, H. Zhao, and N. Liu. (2007). Thermal conductivity of boron nitride reinforced polyethylene composites. *Materials Research Bulletin*, 42(10), 1863-1873.